# A Failure Detection Technique for Au-Plated CMOS Microelectrode Arrays

Xin Zhang, Minghao Li, and Sara S. Ghoreishizadeh
*Department of Electrical and Electronic Engineering, University College London*, London, United Kingdom
Emails: {xin-zhang, minghao.li.19, s.ghoreishizadeh}@ucl.ac.uk

***Abstract*—A method for the detection of failure in gold-plated microelectrodes is presented. Three main failure mechanisms – layer detachment, biofouling and halide-mediated passivation (HMP) – were induced on the microelectrodes, leading to electrode failure. Sequential admittance and sensitivity measurements were carried out on gold-plated microelectrodes on printed circuit boards (PCBs) and CMOS chips to develop and train the classifier. A two-step classifier is proposed that relies only on measuring the admittance magnitude ($|Y|$) at three specific frequencies within 0.6 - 800 Hz. The classifier achieves 88% accuracy on PCB microelectrodes and 92% accuracy on CMOS microelectrodes.**

***Index Terms*—CMOS microelectrode, electrochemical impedance spectroscopy, fault detection**

## I. Introduction

Complementary Metal-Oxide-Semiconductor (CMOS) technology forms the foundation of modern electronic circuits and systems, renowned for its low power consumption, high integration density, and scalability [1]. These attributes have positioned CMOS at the forefront of numerous applications, ranging from microprocessors and memory devices to advanced sensor systems [2]. Notably, the integration of CMOS technology with microelectrode fabrication techniques holds significant promise for developing advanced biosensor platforms [2], [3] that combine sensing electrodes with on-chip signal processing and data acquisition systems to reduce the signal path [4].

Electrochemical techniques are the most prevalent methods employed in biosensors to transduce analyte concentrations into measurable electrical signals, owing to their high sensitivity and label-free detection capabilities [5], [6]. The synergy of CMOS technology and electrochemical biosensors enables precise analyte detection, scalability for parallel sensing [7], low-cost redundancy, and inherent on-site data processing [8]. Over the past decade, CMOS-based electrochemical biosensors have been developed to detect various analytes ranging from cells and proteins to neuronal activities using large microelectrode arrays [6], [7], [9]. Despite these advancements, challenges such as biofouling, passivation, and delamination significantly impact the long-term reliability of electrochemical biosensors when used in complex biological fluids [10]–[14]. The capability to detect failure incidents in-situ is an essential feature to ensure the integrity and reliability of readings from CMOS-integrated microelectrode arrays.

Gold is widely used as a substrate material for electrochemical electrodes due to its excellent electrical conductivity and biocompatibility. However, issues like biofouling and halide-mediated passivation (HMP) have been reported to significantly interfere with the sensitivity and reproducibility of gold electrodes [10], [15]. Biofouling occurs due to the nonspecific adsorption of biomolecules onto the electrode surface, such as proteins, cells, and peptides [13], [14], which blocks analytes from approaching the electrode and impedes charge transfer between the electrode and the solution. HMP leads to the formation of a passivation layer on the electrode surface due to halide ions in the solution [16]–[19]. A partial or total delamination or removal of gold may also happen in gold-plated CMOS microelectrodes, where in particular the plated gold layer is thin (up to a few microns).

Considerable efforts have been made to address and prevent failure throughout the development of electrochemical biosensors. For example, effective electrode surface modifications have been investigated to mitigate biofouling and passivation [20]–[23]. However, surface modifications are only compatible with specific applications, limiting their versatility across diverse biosensor platforms. Moreover, continuous assessment of electrode health is still crucial to ensure the reliability and accuracy of measured data. Previous works demonstrate the application of electrochemical impedance spectroscopy (EIS) alone [24] or combined with machine learning techniques [25] for failure detection in microelectrodes, achieving near 80% prediction accuracy [25]. These have so far used the charge transfer resistance and double-layer capacitance values as main features for the classification, which require measurement of impedance over a wide range of frequencies. We recently demonstrated an alternative classifier that only requires measurements of admittance at a single frequency [10] for gold macroelectrodes.

In this paper, we present an empirically driven two-step classification technique to detect failure in "microelectrodes" based on electrochemical impedance at only a few frequencies. We also propose a circuit to implement the proposed classification on-chip.

This work has been funded by the UCL Knowledge Exchange through project KEI2024-01-26

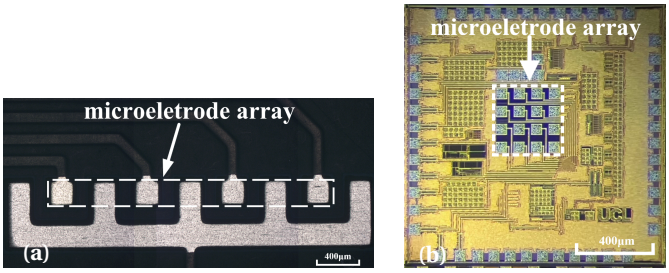

Fig. 1: Micrographs of microelectrodes on (a) PCB (b) CMOS chip

## II. Methods

We initially developed the proposed technique using data derived from PCB microelectrodes before transferring it to CMOS microelectrodes. This was due to the limited availability of CMOS microelectrode samples.

### A. Fabrication of Microelectrodes

The CMOS chip (shown in Fig. 1b) was fabricated in 180 nm CMOS technology at Taiwan Semiconductor Manufacturing Company (TSMC). Sixteen microelectrodes of 66 $\mu$m×66 $\mu$m were implemented on the top metal layer (Al). The Al microelectrodes went through an electroless gold plating process described in [26]. Only two microelectrodes per chip within the array that were directly connected to peripheral pads were used in this work.

The PCB microelectrodes (shown in (Fig. 1a) ) are 200 $\mu$m × 200 $\mu$m and are fabricated at JLCPCB. An electroless nickel immersion gold (ENIG) finish was applied to the electrodes by the manufacturer.

The microelectrodes on both the PCBs (Fig. 1a) and CMOS chips (Fig. 1b) were then electroplated with gold in-house as explained here. The PCB electrodes and CMOS chips were individually immersed in a gold electroplating solution (NB Semiplate Au 100 from NB Technologies GmbH®) for 10 minutes when a pulsed current (at 100Hz, 50% duty cycle) with an average density of 1.5 mA/cm$^2$ was applied between the microelectrode and a platinised Ti counter electrode (from Ti-shop.com). The Au-plated microelectrodes are hereafter referred to as PCB or CMOS electrodes for simplicity. To assess the similarity of the surface of PCB and CMOS electrodes, the surface roughness and composition of the electrodes were measured using AFM (atomic force microscopy) and EDX (energy dispersive X-Ray spectroscopy) respectively. These are reported in Table I showing over 98% gold on both electrodes with surface roughnesses that are statistically similar.

TABLE I: Comparison between PCB and CMOS electrodes

| Microelectrode | Surface Roughness (nm rms) | Gold Composition (%) |
|---|---|---|
| CMOS | 83.6±8.76 | 98.6±0.92 |
| PCB | 76.1±7.45 | 98.5±0.74 |

### B. Failure Induction

We employed our previously reported method for inducing failure [10] on the PCB electrodes. Briefly, electrodes were incubated at 37°C in two groups: in group A electrodes were incubated in PBS, and in mucin protein-enriched PBS in group B.

Three batches of incubation experiments were carried out, containing 26 PCB microelectrodes in total. In the first batch, EIS and sensitivity tests were carried out (on two electrodes at each single time point) at 5, 10, 15, 30, 45, and 60 minutes after incubation. In the second and third batches, four electrodes from each group were incubated for periods ranging from 1 hour up to 4 hours and 36 hours, to assess mid- and long-term incubation effects.

A total of 24 CMOS electrodes were analyzed. This included four freshly prepared and/or healthy electrodes. Due to the limited availability of CMOS electrodes, batch failure induction experiments were impractical. Instead, a total of 20 CMOS microelectrodes that had already failed during our previous studies were used.

### C. PCB Electrode Characterization

EIS measurements were performed before and after incubation in PBS with 5 mM potassium ferri/ferrocyanide. The frequency ranges from 1 MHz to 0.1 Hz, yielding 71 complex impedance values. Electrode performance was characterized using cyclic voltammetry (CV) measurements conducted in 5 mM and 2.5 mM potassium ferri/ferrocyanide solutions. The applied potential ranged from 0 V to 0.4 V, with a scan rate of 0.1 V/s. Sensitivity was defined as the difference in the oxidation peak currents on the two voltammograms divided by the difference in concentration. Electrodes exhibiting sensitivity lower than half that of fresh electrodes were labelled as failed.

A total of 107 measurements were obtained from the PCB electrodes in groups A and B.

## III. Results and Discussion

### A. PCB electrodes

Among the 107 measurements, 55 were obtained from newly electroplated electrodes. These data showed consistent results, with an average initial sensitivity of 327 nA/mM and a standard deviation of 4.8 nA/mM. The threshold for classifying an electrode faulty based on changes in its sensitivity alone was set at half the initial sensitivity, 163 nA/mM. EIS results were analyzed using the Randles equivalent circuit to model the kinetics of electrochemical reactions at the electrode interface. Circuit parameters from new electrodes showed a maximum variation of 6.7%, indicating a relatively low inter-electrode variation.

#### 1) Failure Categories

Out of the 52 data points obtained after incubation, 10 electrodes maintained sensitivities above the threshold (163 nA/mM) and exhibited clear, distinct peaks in CV measurements. These were labelled as healthy. The remaining 42 electrodes were labelled as failed. The analysis of the CV and EIS of these reveals three distinct categories of failure.

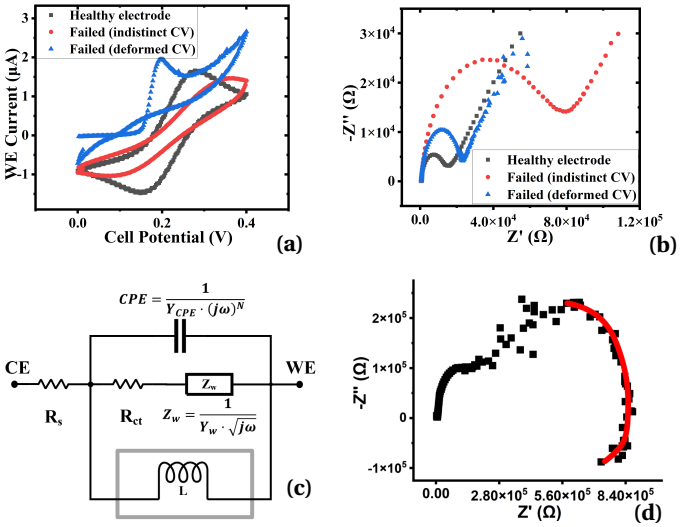


Fig. 2: Examples of (a) CV and (b) EIS measurements on a healthy electrode (black), an electrode with indistinct CV peaks (red), and a deformed CV curve (blue). (c) RC-equivalent circuit of microelectrodes, showing constant phase element ($CPE$), Warburg component ($Z_w$), solution ($R_s$), charge transfer resistance ($R_{ct}$), and an inductance $L$. (d) Example Nyquist plot of a faulty microelectrode where impedance values fluctuate and an inductance effect appears, highlighted by a red semicircle.

(I) Low Sensitivity - This is directly seen from the decreased peak current in an otherwise normal-looking cyclic voltammogram. This coexists with an increased charge transfer resistance ($R_{ct}$). The increase in $R_{ct}$ indicates hindered charge exchange between the electrode and the solution that can be attributed to adsorbed materials or to the formation of passivation layers on the electrode surface that reduce the effective electrode area.

(II) Indistinct CV Peaks - where the oxidation and reduction peaks do not appear anymore in the CV, as shown in red voltammogram in Fig. 2a. This is accompanied by a decrease in the constant phase element (CPE) factor $N$. It decreases from an average of 0.98, observed in new electrodes as well as the other two types of faulty electrodes, to below 0.7. indicating deviation from ideal capacitive behaviour. Smaller N values lead to a current, which is proportional to the applied voltage, interfering the faradic peak current in CV. This phenomenon is likely due to the inhomogeneities of the double-layer structure induced by the non-uniform biofouling and passivation layer, which lead to a distribution of capacitive elements with different time constants. [27], [28].

(III) Deformed CV - where CV displays distorted peaks with the anodic and cathodic scans being asymmetric and crossing over. One example is shown in the blue voltammogram in Fig. 2a. It was observed that the deformations in the CV were always accompanied by fluctuations in the low-frequency range of EIS, an example of which is as shown in Fig. 2b. There was a total of 9 electrodes with deformed CV. Three of these also showed a clear inductive behaviour as shown in Fig. 2d. The inductive behaviour indicates a Volmer-Heyrovsky mechanism involving adsorption and desorption processes [29]. This behaviour aligns with HMP processes where halide ions first adsorb to the gold surface, then electrochemically react with gold, and finally, the gold complex desorbs from the electrode [16]. Another possible mechanism contributing to the inductive behaviour is the light-triggered reaction between gold and potassium ferri/ferrocyanide [9], which electrochemically etches gold. It should be noted that although the inductive behaviour does not intrinsically lead to fluctuation in low-frequencies, the formation of the non-uniform passivation layer and the delamination caused by etching can lead to fluctuation in the pseudo-inductance.

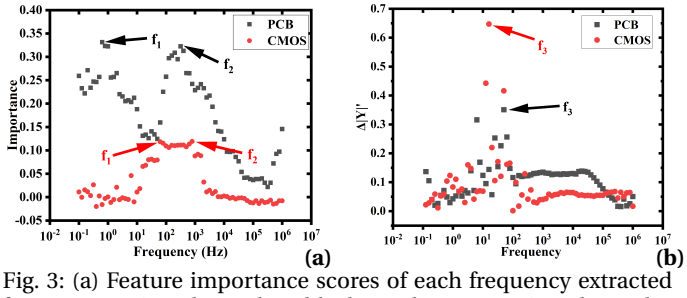


Fig. 3: (a) Feature importance scores of each frequency extracted from PCB microelectrodes (black) and CMOS microelectrodes (red). (b) The average $\Delta|Y|_N$ derived from all fluctuating electrodes on PCB and CMOS.

*2) Detection of Failure*

Since the variations in $R_{ct}$ and $N$ significantly affect the impedance, the associated failures can be detected by measuring the admittance magnitude ($|Y|$). However, failures that involve impedance fluctuation are difficult to detect by simple threshold comparisons. Therefore, a two-step classification approach is proposed.

*3) First-Step Classification*

All obtained EIS data were first labelled as (I) healthy or (II) faulty without fluctuating EIS (WOFE) and (III) faulty with fluctuating EIS (WFE). Those in the WFE group were excluded. To assess the importance of each frequency in predicting failure, a total of 71 $|Y|$ values measured at frequencies from 0.1 Hz to 1 MHz were used to train 10,000 random forest classifiers. The results plotted in Fig. 3a show two frequencies, 0.6 Hz and 300 Hz, to be most significant. The decision tree classifier was then trained with different numbers of features (i.e. impedance measured at a single frequency) starting with the most important frequencies. Training was done on 80% of the data and validating on the remaining 20% plus all fluctuating measurements. We found that using only the top two frequencies provides good classification accuracy. Using a few more frequencies will only increase the accuracy by less than 1% while using higher than five frequencies decreases the accuracy because the less important frequencies are less related to the health state. since accuracy does not significantly improve with the addition of more frequencies. The threshold values for these two features were determined by averaging specific decision thresholds

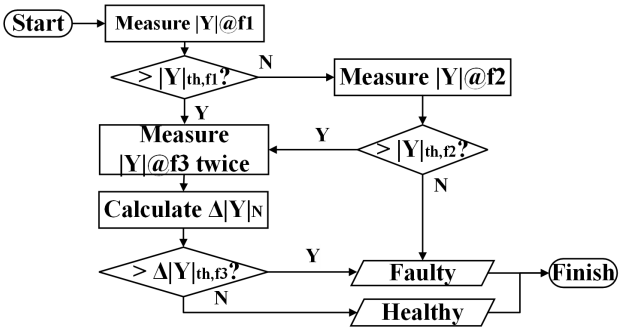


Fig. 4: Flowchart of the two-step classification

over all trained decision trees with these two features. The accuracy of the classification was assessed with all 107 measurements and found to be 83%.Notably, while 87% of healthy and WOFE electrodes were correctly classified, only 44% of the WFE were correctly detected in this step. A second step classification was therefore designed to improve the detection of WFE electrodes.

*4) Second-Step Classification*

The variation in repeat admittance measurement at a single frequency, $f_3$, is found to be an effective feature in detecting WFE electrodes. This is calculated using the following equation:

$$\Delta|Y|_N = |\frac{|Y|_{@f_3,2} - |Y|_{@f_3,1}}{\min(|Y|_{@f_3,1}, |Y|_{@f_3,2})}| \quad (1)$$

where $|Y|_{@f_3,1}$ and $|Y|_{@f_3,2}$ are the magnitudes of the admittances measured at $f_3$ the first and second times, respectively. The frequency, $f_3$ was selected where the variation of the admittance is maximum. This was found by calculating the average normalised difference between admittance at adjacent frequencies among all WFE electrodes. The average and standard deviation of $\Delta|Y_{f_3}|_N$ were found to be 0.07 ± 0.008 $\Omega^{-1}$, and 0.35 ± 0.14 $\Omega^{-1}$ for the healthy and WFE electrodes, respectively. A threshold of 0.2 $\Omega^{-1}$ was therefore selected. This step achieved 100% accuracy in detecting WFE electrodes, improving the overall classifier accuracy to 87.9%. The two-step classifier in summarised in a flowchart in Fig. 4, with the parameters extracted from the trained decision tree listed in Table II:

TABLE II: Optimized Classifier Parameters

| Parameter (Units) | PCB Microelectrode | CMOS Microelectrode |
|---|---|---|
| $f_1$ (Hz) | 0.6 | 60 |
| $f_2$ (Hz) | 300 | 800 |
| $f_3$ (Hz) | 50 | 15 |
| $\|Y\|_{th,f_1}$ (S) | $1.12\times10^{-5}$ | $1.64\times10^{-4}$ |
| $\|Y\|_{th,f_2}$ (S) | $5.87\times10^{-5}$ | $8.11\times10^{-4}$ |
| $\Delta\|Y\|_{th,f_3}$ | 0.2 | 0.2 |
| Accuracy | 88% | 92% |

## B. CMOS electrodes

With only 24 measurements from the CMOS chips, retraining the classifier was infeasible. Instead, a data scaling technique was implemented, to generate synthetic data from the healthy PCB electrodes (overall 65 electrodes).To do this, the $R_{ct}$, $CPE$ and $Z_w$ of the PCB electrodes were firstly estimated from the impedance information. These were then scaled using the ratio of the areas of the PCB and CMOS electrodes, $\left(\frac{200\mu m}{66\mu m}\right)^2$ to obtain equivalent values in the CMOS electrode size. $R_{ct}$ and $CPE$ are proportional to $\frac{1}{A}$ while the Warburg impedance, $Z_w$ is proportional to $\frac{1}{\sqrt{A}}$). The obtained values agree with the EIS measured from the newly fabricated CMOS microelectrode, which proves the viability of the method.

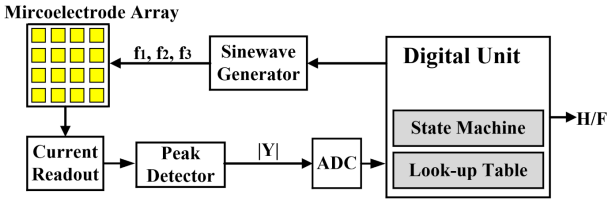


Fig. 5: Circuit implementation of fault detection technique. (H/F: Healthy/Faulty)

The EIS data from faulty PCB electrodes are not suitable for conversion due to relatively high errors in extracting the circuit parameters using circuit fitting. The 65 synthetic and 24 CMOS measurements were used to train the CMOS classifier following the same procedure as PCB electrodes. The main parameters of the classifier are listed in Table II. The classifier achieved 87.5% accuracy in the first step. This is improved to 91.7% after the second step.

## C. Circuit Implementation

A simplified block diagram of a circuit to implement the proposed 2-step classification is presented in Fig. 5. The circuit includes an excitation signal generator (potentially implemented using a direct digital synthesizer) that sequentially produces sine waves at the three critical frequencies with a small amplitude (typically 10 mV), with a current readout circuit followed by a peak detector to measure the amplitude of electrode current, which is a scaled version of $|Y|$. Further experiments are planned with the sensors to identify the maximum acceptable voltage step in the sine wave. The decision tree can be implemented through a mix of digital and analogue blocks or a fully digital circuit that includes a digital state machine, a look-up table and digital comparators. The majority of the analogue and data converter circuits can be shared with the amperometric readout circuit which substantially reduces the overhead of the classifier.

# IV. Conclusion

A two-step failure detection technique for gold-plated CMOS microelectrodes is presented that achieves 92% accuracy. The classifier detects electrodes with decreased sensitivity or deformed CV curves by measuring admittance at three specific frequencies and comparing them with set thresholds. The proposed electrode classification technique can be easily implemented on-chip with minimal overhead compared to alternative techniques. Future work includes expanding the classifier to dynamically adjust parameters for long-term monitoring.

## REFERENCES


[1] X. Liu, L. Li, B. Awate, R. M. Worden, G. Reguera, and A. J. Mason, "Biosensor array microsystem on a cmos amperometric readout chip," ser. Biomedical Circuits and Systems Conference, 2011, pp. 305–308.

[2] S. Joo and R. B. Brown, "Chemical sensors with integrated electronics," *Chemical Reviews*, vol. 108, no. 2, pp. 638–651, FEB 2008.

[3] A. A. S. Gill and S. S. Ghoreishizadeh, "Advances in nanomaterials integration in cmos-based electrochemical sensors: A review," *IEEE Sensors Journal*, vol. 23, no. 5, pp. 4659–4671, MAR 1 2023.

[4] L. Li, H. Yin, A. J. Mason, L. Li, H. Yin, and A. J. Mason, "Epoxy chip-in-carrier integration and screen-printed metalization for multi-channel microfluidic lab-on-cmos microsystems," *IEEE Transactions on Biomedical Circuits and Systems.*, vol. 12, no. 2, pp. 416–425, 2018-4.

[5] S. S. Ghoreishizadeh, I. Taurino, G. De Micheli, S. Carrara, and P. Georgiou, "A differential electrochemical readout asic with heterogeneous integration of bio-nano sensors for amperometric sensing," *IEEE Transaction ON Biomedical Circuits and Systems*, vol. 11, no. 5, pp. 1148–1159, OCT 2017.

[6] M. Vestergaard, K. Kerman, and E. Tamiya, "An overview of label-free electrochemical protein sensors," *Sensors*, vol. 7, no. 12, pp. 3442–3458, DEC 2007.

[7] M. Li, A. Vanhoestenberghe, and S. S. Ghoreishizadeh, "An integrated circuit to enable electrodeposition and amperometric readout of sensing electrodes," 2022, pp. 85–88, 13th Latin America Symposium on Circuits and System (LASCAS), Puerto Varas, Chile, APR 01-04, 2022.

[8] B. Eversmann, M. Jenkner, F. Hofmann, C. Paulus, R. Brederlow, B. Holzapfl, P. Fromherz, M. Merz, M. Brenner, M. Schreiter, R. Gabl, K. Plehnert, M. Steinhauser, G. Eckstein, D. Schmitt-Landsiedel, and R. Thewes, "A 128x128 cmos biosensor array for extracellular recording of neural activity," *IEEE Journal of Solid-State Ccircuits*, vol. 38, no. 12, pp. 2306–2317, DEC 2003.

[9] L. Li, X. Liu, W. A. Qureshi, and A. J. Mason, "Cmos amperometric instrumentation and packaging for biosensor array applications," *IEEE Transcations on Biomedical Circuits and Syetems*, vol. 5, no. 5, pp. 439–448, OCT 2011.

[10] X. Zhang and S. S. Ghoreishizadeh, "Detecting deterioration in electrochemical sensing au electrodes with admittance measurement," *IEEE Biosensors Conference*, 2024.

[11] N. Wisniewski and M. Reichert, "Methods for reducing biosensor membrane biofouling," *Colloids and Surfaces.*, vol. 18, no. 3-4, pp. 197–219, 2000.

[12] J. Kuhlmann, L. Dzugan, and W. Heineman, "Comparison of the effects of biofouling on voltammetric and potentiometric measurements," *Electroanalysis*, vol. 24, no. 8, pp. 1732–1738, 2012.

[13] N. Wisniewski, F. Moussy, and W. Reichert, "Characterization of implantable biosensor membrane biofouling," *Fresenius' Journal of Analytical Chemistry*, vol. 366, no. 6-7, pp. 611–621, 2000.

[14] M. KYROLAINEN, P. RIGSBY, S. EDDY, and P. VADGAMA, "Biocompatibility hemocompatibility - implications and outcomes for sensors," *Acta Anaesthesiologica Scandinavica.*, vol. 39, pp. 55–60, 1995.

[15] A. N. Naeem and S. S. Ghoreishizadeh, "False sensitivities in cortisol immunosensors fabricated on gold-screen-printed electrodes," *IEEE Biosensors Conference*, 2024.

[16] A. J. Bard, L. R. Faulkner, and H. S. White, *Electrochemical methods: fundamentals and applications*. John Wiley & Sons, 2022.

[17] O. Kasian, N. Kulyk, A. Mingers, A. R. Zeradjanin, K. J. J. Mayrhofer, S. Cherevko, O. Kasian, N. Kulyk, A. Mingers, A. R. Zeradjanin, K. J. Mayrhofer, and S. Cherevko, "Electrochemical dissolution of gold in presence of chloride and bromide traces studied by on-line electrochemical inductively coupled plasma mass spectrometry," *Electrochimica Acta*, vol. 222, pp. 1056–1063, 2016-12.

[18] J. Ribeiro, E. Silva, and C. Pereira, "Electrochemical characterization of redox probes at gold screen-printed electrodes: Efforts towards signal stability," *ChemistrySelect.*, vol. 5, no. 17, pp. 5041–5048, 2020.

[19] X. Xu, A. Makaraviciute, and Z. Zhang, "Revisiting the factors influencing gold electrodes prepared using cyclic voltammetry," *Sensors and Actuators.*, vol. 283, pp. 146–153, 2019.

[20] L. Zhou, X. Li, B. Zhu, and B. Su, "An overview of antifouling strategies for electrochemical analysis," *Electroanalysis*, vol. 34, no. 6, pp. 966–975, 2022.

[21] T. Xiao, F. Wu, J. Hao, M. Zhang, P. Yu, and L. Mao, "In vivo analysis with electrochemical sensors and biosensors," *Analytical Chemistry*, vol. 89, no. 1, pp. 300–313, 2017.

[22] M. Zhang, P. Yu, and L. Mao, "Rational design of surface/interface chemistry for quantitative in vivo monitoring of brain chemistry," *Accounts of Chemical Research*, vol. 45, no. 4, pp. 533–543, 2012.

[23] P.-H. Lin and B.-R. Li, "Antifouling strategies in advanced electrochemical sensors and biosensors," *The Analyst Online /*, vol. 145, no. 4, pp. 1110–1120, 2020.

[24] S. S. Ghoreishizadeh, X. Zhang, S. Sharma, and P. Georgiou, "Study of electrochemical impedance of a continuous glucose monitoring sensor and its correlation with sensor performance," *IEEE Sensors Letters.*, vol. 2, no. 1, 2018.

[25] H. Sharma, D. Kalita, and K. Mirza, "Prediction of glucose sensor sensitivity in the presence of biofouling using machine learning and electrochemical impedance spectroscopy," *IEEE Sensors Journal.*, vol. 23, no. 16, pp. 18 785–18 797, 2023.

[26] M. Li, A. N. Naeem, H. T. Lancashire, A. Vanhoestenberghe, and S. S. Ghoreishizadeh, "Electroless au plating of cmos microelectrodes: Fabrication, characterization, and electrochemical measurement," *IEEE Sensors Letters*, vol. 8, no. 6, JUN 2024.

[27] C. Hsu and F. Mansfeld, "Technical note: Concerning the conversion of the constant phase element parameter y0 into a capacitance," *Corrosion*, vol. 57, no. 9, pp. 747–748, SEP 2001.

[28] G. BRUG, A. VANDENEEDEN, M. SLUYTERSREHBACH, and J. SLUYTERS, "The analysis of electrode impedances complicated by the presence of a constant phase element," *Journal of Electroanalytical Chemistry*, vol. 176, no. 1-2, pp. 275–295, 1984.

[29] A. Lasia, "Mechanism and kinetics of the hydrogen evolution reaction," *International Journal of Hydrogen Energy*, vol. 44, no. 36, pp. 19 484–19 518, JUL 26 2019.